ISSN 1726-5749

SENSORS & TRANSDUCERS

12/08
vol. 3
Special

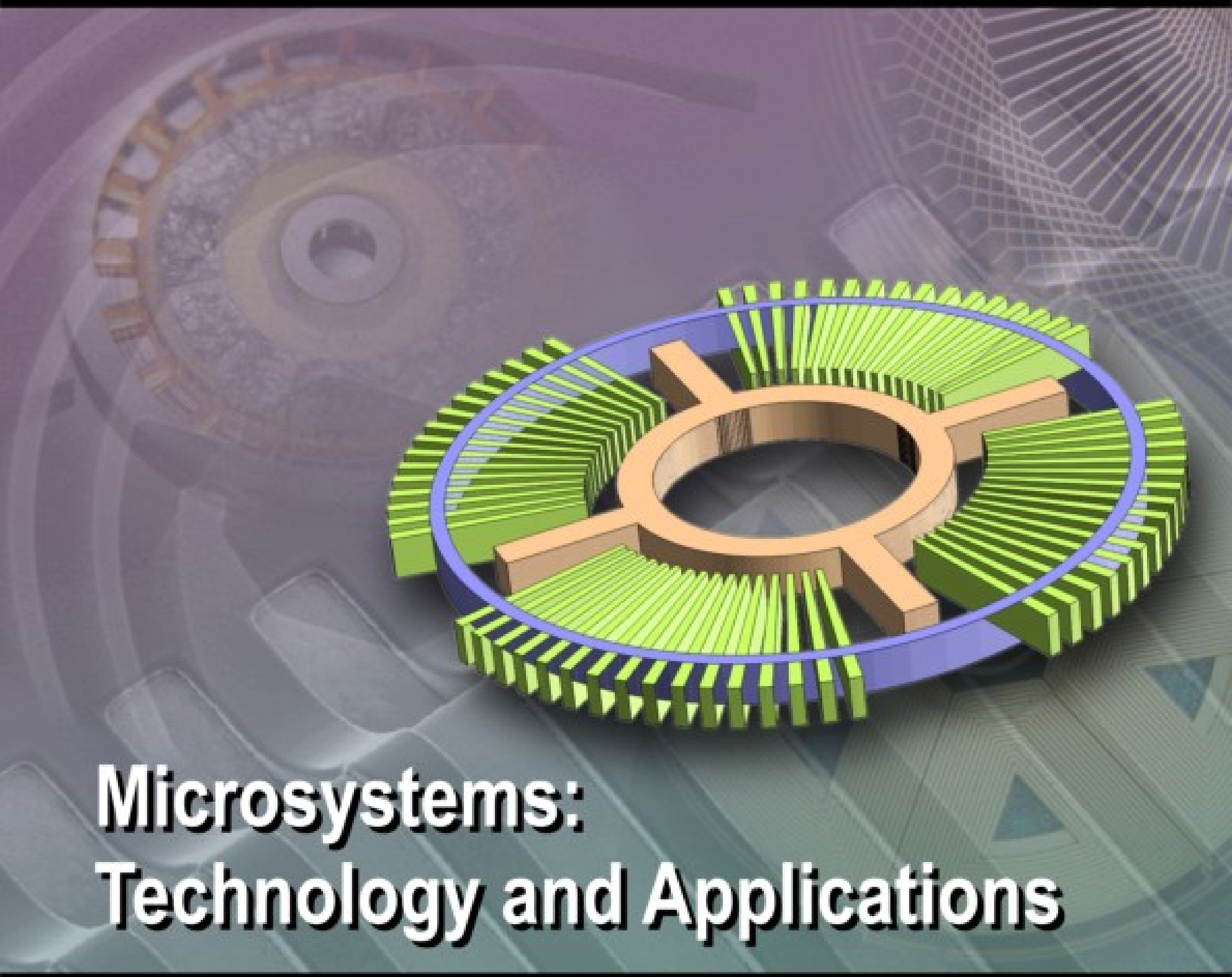

Microsystems: Technology and Applications

International Frequency Sensor Association Publishing

IFSA

Sensors & Transducers

Volume 3
Special Issue
December 2008

www.sensorsportal.com

ISSN 1726-5479

Sensors & Transducers Journal (ISSN 1726-5479) is a peer review international journal published monthly online by International Frequency Sensor Association (IFSA).
Available in electronic and CD-ROM.

Sensors & Transducers Journal

Contents

Volume 3
Special Issue
December 2008

www.sensorsportal.com

ISSN 1726-5479

Research Articles

Foreword
Elena Gaura and James Brusey 1

Novel Synchronous Linear and Rotatory Micro Motors Based on Polymer Magnets with Organic and Inorganic Insulation Layers
Andreas Waldschik, Marco Feldmann and Stephanus Büttgenbach 3

Adaptive Subband Filtering Method for MEMS Accelerometer Noise Reduction
Piotr Pietrzak, Barosz Pekoslawski, Maciej Makowski, Andrzej Napieralski 14

Fluido-Dynamic and Electromagnetic Characterization of 3D Carbon Dielectrophoresis with Finite Element Analysis
Rodrigo Martinez-Duarte, Salvatore Cito, Esther Collado-Arredondo, Sergio O. Martinez and Marc J. Madou 25

Membranous Bypass Valves for Discrete Drop Mixing and Routing in Microchannels
Minsoung Rhee and Mark A. Burns 37

Ultrasound-driven Viscous Streaming, Modelled via Momentum Injection
James Packer, Daniel Attinger and Yiannis Ventikos 47

Multi-Functional Sensor System for Heart Rate, Body Position and Movement Intensity Analysis
Michael Mao, Bozena Kaminska, Yindar Chuo 59

NIR FRET Fluorophores for Use as an Implantable Glucose Biosensor
Majed Dweik and Sheila A. Grant 71

Electrostatic Voltage Sensors Based on Micro Machined Rotational Actuators: Modeling and Design
Jan Dittmer, Rolf Judaschke and Stephanus Büttgenbach 80

Optimization of Phage-Based Magnetoelastic Biosensor Performance
S. Huang, S.-Q. Li, H. Yang, M. Johnson, J. Wan, I. Chen, V. A. Petrenko, J. M. Barbaree, and B. A. Chin 87

Contribution of NIEL for Gain Degradation (β) in Si^{8+} Ion Irradiated Silicon Power Transistor
C. M. Dinesh, Ramani, M. C. Radhakrishna, S. A. Khan, D. Kanjilal 97

Sensors & Transducers Journal, Vol. 3, Special Issue, December 2008, pp. 47-58

www.sensorsportal.com

Sensors & Transducers

ISSN 1726-5479

http://www.sensorsportal.com

Ultrasound-driven Viscous Streaming, Modelled via Momentum Injection

[1]James PACKER, [2]Daniel ATTINGER and [1]Yiannis VENTIKOS
[1]Fluidics and Biocomplexity Group, Department for Engineering Science,
University of Oxford, Oxford, OX1 3PJ, UK
Tel.: +44(0)1865-283452
[2]Laboratory for Microscale Transport Phenomena,
Department of Mechanical Engineering, Columbia University, tel.: +1 212 854 28 41
E-mail: Yiannis.Ventikos@eng.ox.ac.uk, da2203@columbia.edu

Received: 31 October 2008 /Accepted: 7 November 2008 /Published: 8 December 2008

Abstract: Microfluidic devices can use steady streaming caused by the ultrasonic oscillation of one or many gas bubbles in a liquid to drive small scale flow. Such streaming flows are difficult to evaluate, as analytic solutions are not available for any but the simplest cases, and direct computational fluid dynamics models are unsatisfactory due to the large difference in flow velocity between the steady streaming and the leading order oscillatory motion. We develop a numerical technique which uses a two-stage multiscale computational fluid dynamics approach to find the streaming flow as a steady problem, and validate this model against experimental results. *Copyright © 2008 IFSA.*

Keywords: Acoustic streaming, CFD, Lab-on-a-chip, Microfluidic devices, Multiscale

1. Introduction

In addition to the first order oscillating flow generated by a gas bubble in a fluid excited by ultrasound pressure waves, a steady second order flow is generated, [1], [2]. This is difficult to model with standard computational fluid dynamics (CFD) techniques, due to the difference in time scales exhibited by the first order oscillating flow (O(kHz) or higher) and the steady second order flow (O(10Hz)) in the configurations considered. Were the second order flow to be determined by standard transient CFD modelling, many thousands of cycles would need to be calculated to determine the nature of the steady flow with reasonable accuracy, as the magnitude of the steady flow is many orders lower than that of the first order oscillating flow.

In this paper, a novel technique for modelling this steady flow is proposed, where the flow is considered to have two parts, the steady second order flow and the time-varying first order flow. In this technique the first order flow is found directly with a CFD modelling technique, and the flow properties are used to calculate the forcing which drives the second order flow. This second order flow is then modelled as a steady state CFD problem, using the calculated forcing to drive the model.

2. Computational Fluid Dynamics Modelling

2.1. First Order

The first order model involves a standard CFD approach, where the flow is excited by a moving boundary. In this paper the case of a hemispherical bubble in water is considered, where the bubble wall is displaced sinusoidally, modelling periodic volumetric oscillation. The first order simulation is transient, with three full periods of oscillation modelled. This allows post-transient conditions to be reached, confirmed by comparing the results of the second and third period.

2.2. Second Order

The second order CFD model predicts the steady streaming expected for the configuration chosen. The geometric model used is the same as that for the first order, but is established within a steady flow model: The moving bubble wall is not modelled, and replaced in the simulation with a static boundary at the mean position. To excite the steady streaming flow, forcing terms are calculated from the first order flow, and added to the fluid volume, as momentum sources, in the region where a viscous sub-layer would exist. The method of calculation of the forcing and the layer thickness is outlined below.

3. Calculation of Forcing

3.1. Theory

The momentum injection is calculated following the analysis of Lighthill, [3], finding the forcing from the gradients of the Reynolds stresses. The techniques used have been developed to describe turbulent flow, but are equally applicable to the flow considered, as both flow types have constant and time varying flow components interacting. The Reynolds decomposition allows the constant and time varying flow parts to be considered separately, with the time varying first order flow driven by the oscillating boundary conditions, and the steady second order flow driven by the Reynolds stresses, which are calculated using the first order flow velocities. If *u, v* and *w* are the first order flow velocities in the three Cartesian directions, ρ the fluid density, $F_{u,v,w}$ is the force per unit volume caused by the Reynolds stresses and driving the steady second order flow in the three Cartesian directions, and is given by:

$$F_u = -\rho\left(\frac{\partial \overline{uu}}{\partial x} + \frac{\partial \overline{uv}}{\partial y} + \frac{\partial \overline{uw}}{\partial z}\right) \tag{1}$$

$$F_v = -\rho\left(\frac{\partial \overline{vu}}{\partial x} + \frac{\partial \overline{vv}}{\partial y} + \frac{\partial \overline{vw}}{\partial z}\right) \tag{2}$$

$$F_w = -\rho\left(\frac{\partial \overline{wu}}{\partial x} + \frac{\partial \overline{wv}}{\partial y} + \frac{\partial \overline{ww}}{\partial z}\right) \tag{3}$$

Therefore, the mean values over one complete cycle of *u.u, u.v, u.w, v.v, v.w* and *w.w* are found for each cell. The differentials of these mean values must then be found in order to find the forcing. Once the differentials are known, as covered in section 3.2.2, the forcing can be calculated for each cell by adding the three appropriate partial differentials.

This forcing only affects the viscous sub-layer adjacent to the boundary [4], [5], as outside this layer the forcing is absorbed into a hydrostatic pressure field [5]. Different authors give slightly different approximations to the thickness of this viscous layer, with Marmottant *et. al.* [4] giving the thickness as:

$$\delta = \left(\frac{\mu}{\rho \omega} \right)^{\frac{1}{2}} \tag{4}$$

and Lee & Wang [5] as:

$$\delta = \left(\frac{2\mu}{\rho \omega} \right)^{\frac{1}{2}} \tag{5}$$

Here δ is the thickness, μ the absolute viscosity, ω the excitation frequency and ρ the fluid density. Recalling that both expressions are approximations, the difference is not considered significant. In this paper, Marmottant *et. al.*'s [4] approximation is used. In section 4.3 of this publication, the accuracy of this approximation is analyzed further.

3.2. Numerical Techniques

3.2.1. Mean Values

From the first order model, the flow velocities *u, v* and *w* of each cell in the volume around the bubble wall are found at each time-step for one complete period of oscillation, once post-transient conditions have been reached. For each cell, the values of *u.u, u.v, u.w, v.v, v.w* and *w.w* are computed and their mean value is estimated for the complete period.

Therefore values of each mean multiple $\left(\overline{u\,.\,u}\,,\,\overline{u\,.\,v}\,,\,\ldots\right)$, are known at the centre of each cell. These can be treated as scattered data points, for which the differentials in the *x, y* and *z* directions are needed.

3.2.2. Numerical Differentiation

In order to find the differentials of the mean values at each location, the approach taken is to find the difference in value and difference in position for three surrounding points, and to find the Cartesian partial derivatives from this by solving the set of three equations of the form:

$$\delta V = \delta x \,\frac{\partial V}{\partial x} + \delta y \,\frac{\partial V}{\partial y} + \delta z \,\frac{\partial V}{\partial z}\,, \tag{6}$$

where V is the relevant value to be differentiated $\left(\overline{u\,.\,u}\,,\,\overline{u\,.\,v}\,,\,\ldots\right)$. As we know three sets of

$(\delta V, \delta x, \delta y, \delta z)$ we can solve at each point for $\left(\frac{\partial V}{\partial x}, \frac{\partial V}{\partial y}, \frac{\partial V}{\partial z}\right)$.

We achieve this by solving the equation:

$$\begin{pmatrix} \frac{\partial V}{\partial x} \\ \frac{\partial V}{\partial y} \\ \frac{\partial V}{\partial z} \end{pmatrix} = \begin{pmatrix} \delta x_1 & \delta y_1 & \delta z_1 \\ \delta x_2 & \delta y_2 & \delta z_2 \\ \delta x_3 & \delta y_3 & \delta z_3 \end{pmatrix}^{-1} \begin{pmatrix} \delta V_1 \\ \delta V_2 \\ \delta V_3 \end{pmatrix}, \tag{7}$$

where the subscripts 1,2 and 3 refer to the values for the three surrounding points chosen. If the three points chosen are nearly collinear or coplanar, this will lead to an ill-conditioned solution. Consequently the solution is found by selecting the three points in close proximity which give a well-conditioned behaviour. The closest 15 points are found and the best combination of three selected. This is found by considering all possible combinations, and finding a parameter which describes the quality of the solution. First the condition number of the matrix

$$\begin{pmatrix} \delta x_1 & \delta y_1 & \delta z_1 \\ \delta x_2 & \delta y_2 & \delta z_2 \\ \delta x_3 & \delta y_3 & \delta z_3 \end{pmatrix}, \tag{8}$$

is found for all possible combinations of three of the close points, here referred to by the subscripts 1, 2, 3. The higher this condition number, the more poorly conditioned the set of equations is. This is then multiplied by the product of the distances to the three points under consideration. The combination with the lowest value of this parameter is chosen, as it is the best-conditioned set of points closest to the point at which the differential is required. This technique is an approximate method of differentiation, which can be applied to any arbitrary three dimensional data set.

The differentiation method is essentially a forwards difference method, extended to three dimensions and applied to a scattered data field.

3.2.3. Forcing

Once the differentials of the mean values $(\overline{u.u}, \overline{u.v}, \ldots)$ are known for each cell in the viscous sub-layer region, the forcing can be found from equations 1, 2 and 3. The forcing is then used in the second order steady-state CDF model as a momentum injection to force the steady streaming. The forcing for each cell is used within the *CFD-ACE2007 solver* (ESI Group, Paris, France) package, in which the forcing per unit volume for each forced cell is multiplied by the cell volume to find the absolute force, and this force used in the equilibrium equations used by the solver, allowing the streaming flow to be computed.

4. Validation

The numerical modelling technique proposed is tested against the experimental results of Tho *et. al.* [1], as their results give both the streaming generated and the bubble motion for different modes of bubble oscillation. Tho *et. al.*'s experimental conditions correspond to a bubble of mean radius varying between 202 and 274 μm. Several modes of bubble vibration are examined, with case 4 being pure volume oscillation of the bubble. This is the case we chose to present in this paper.

4.1. Tho *et. al.*'s Case

4.1.1. Grid

Tho *et. al.*'s experimental volume is a thin chamber, of height 0.66 mm, as described in Fig. 1, Tho *et. al.*, [1]. The hemispherical bubble is on the top wall. Only the region near the bubble is used for our CFD modelling to make the problem more tractable. The grid used is shown in Fig. 1. The grid is divided into different volumes so that the required velocities can be output from the first order model, and the forcing applied only to the viscous sub-layer adjacent to the bubble wall in the second order model. These zones are shown in Fig. 2.

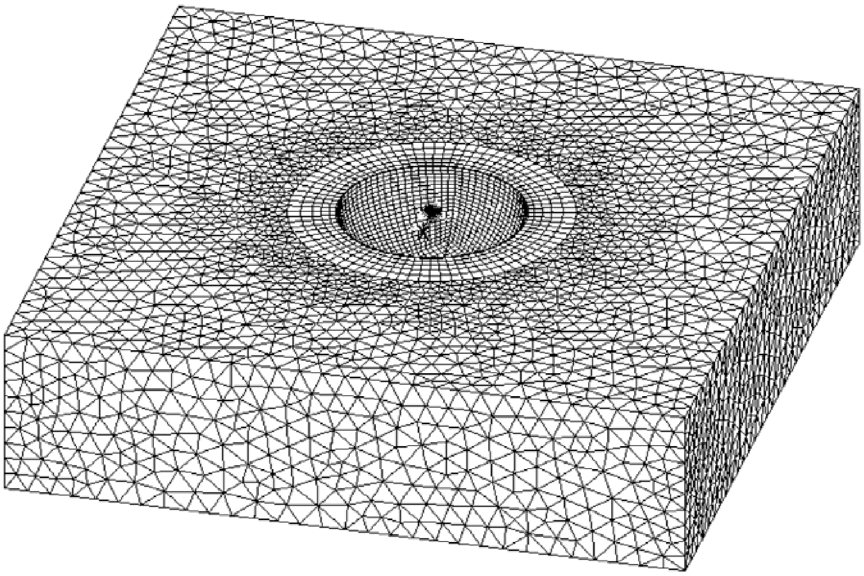

Fig. 1. CFD grid.

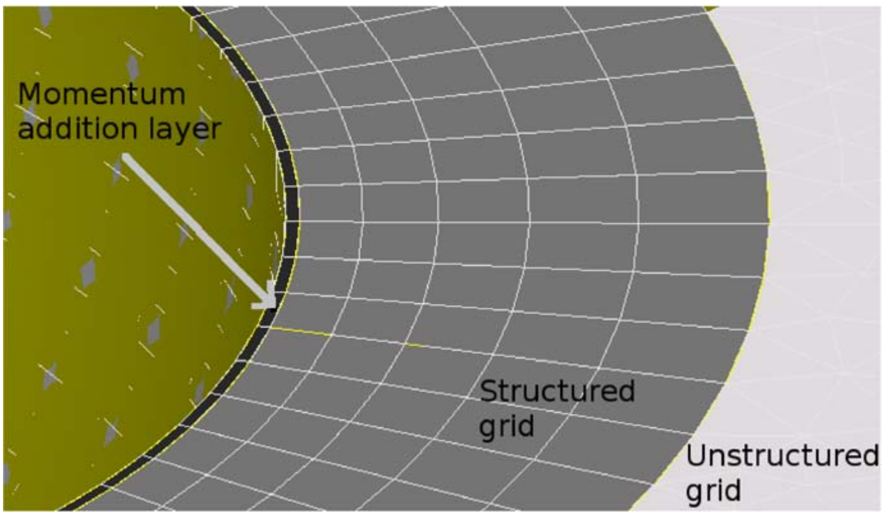

Fig. 2. Grid detail.

4.1.2. Boundary Conditions

In the first order model, the hemispherical bubble is of radius 270 μm, and the bubble wall is oscillated at 8.658 kHz, with a magnitude of 1.41% of the bubble radius, corresponding to case 4 in Tho *et. al.*'s experiments [1]. The boundary condition at the bubble wall is taken as zero slip, since the particles used in the flow visualization congregate at the interface and allow little slip flow [1]. For comparison a model is also computed for zero shear at the bubble wall, which would be expected for perfectly pure fluid, neglecting the viscosity of the bubble gas. The other boundary conditions are the same for the two cases. If the bubble is on the top surface, the top and bottom surfaces have wall boundary conditions (zero tangential and normal flow velocity) and the four edges have fixed pressure boundary conditions, allowing flow between the volume modelled and the large microchamber used experimentally.

4.1.3. Convergence to Post-transient Conditions

For the first order model, 90 time steps are used per period, and three complete periods modelled. To ensure that the model has reached post-transient conditions, the results of period 2 and 3 are compared and found to be essentially similar, with an average difference of 0.11 % between velocities at equivalent time steps within the period.

4.1.4. Data Processing

The flow velocities *u, v, w* are found for the volume adjacent to the bubble (the viscous sub-layer volume) and the cells immediately adjacent to this. From the velocity values for the final period (timesteps 181-270), the forcing in the viscous sub-layer is calculated numerically, following the analysis described above. All calculations were undertaken with *Octave 2.9 & 3.0* (The GNU Project, Boston, USA). Due to the grid deformation in the first order model, the position of the cell centres in the layer vary through the period, so their mean positions are used.

4.1.5. Second Order Model

The same grid and boundary conditions are used for the second order simulation as for the first order transient run, except that the run is steady-state and the bubble wall is maintained in its mean position. The forcing for each cell is added to the viscous sub-layer volume in the simulation, and is the only forcing applied.

4.1.6. Results and Discussion

In Tho *et. al.*'s experimental work, the flow velocities are found by a micro-particle image velocimetry (PIV) technique [1]. Tho *et. al.*'s work measures the flow in three planes parallel to the wall on which the bubble is located, which are referred to as the z_1 plane, through the bubble and 75 μm from the wall, the z_2 plane which is 300 μm from the wall and the z_3 plane which is 525 μm from the wall.

Both the velocities predicted in the numerical model, and observed in Tho *et. al.*'s experiment for the volume oscillation case are shown in Table 1. The velocities are seen to be correct to within one order of magnitude, and the accuracy of the predicted flow velocity is better away from the bubble interface. This may be because the PIV method does not pick up the high velocity flow in the small region immediately adjacent to the bubble, as suggested by Tho *et. al*. in section 4.1 [1].

Table 1. Comparison of numerical and experimental results. Velocities in *mm/s*.

Maximum velocity in plane (mm/s):	Numerical	Tho *et. al.* observed
z_1 plane	1.1	0.3
z_2 plane	0.4	0.3
z_3 plane	0.5	0.3

The pattern of flow predicted by our model, shown in Figs. 3 and 4 for the z_1 and z_2 planes is not identical to the volume oscillation mode of the bubble observed by Tho *et. al.* in their Fig. 15 [1], but does show interesting similarity with that observed for other modes of vibration, including his case 1 (translating oscillation along a single axis), shown in his Fig. 7 [1].

A numerical model was also run simulating free-slip conditions at the bubble wall. This gave velocities of an order of magnitude higher than those observed by Tho *et. al.*, suggesting that the assumption of zero slip at the bubble wall due to particle contamination is valid, and a free-slip model invalid for a particle-bearing fluid.

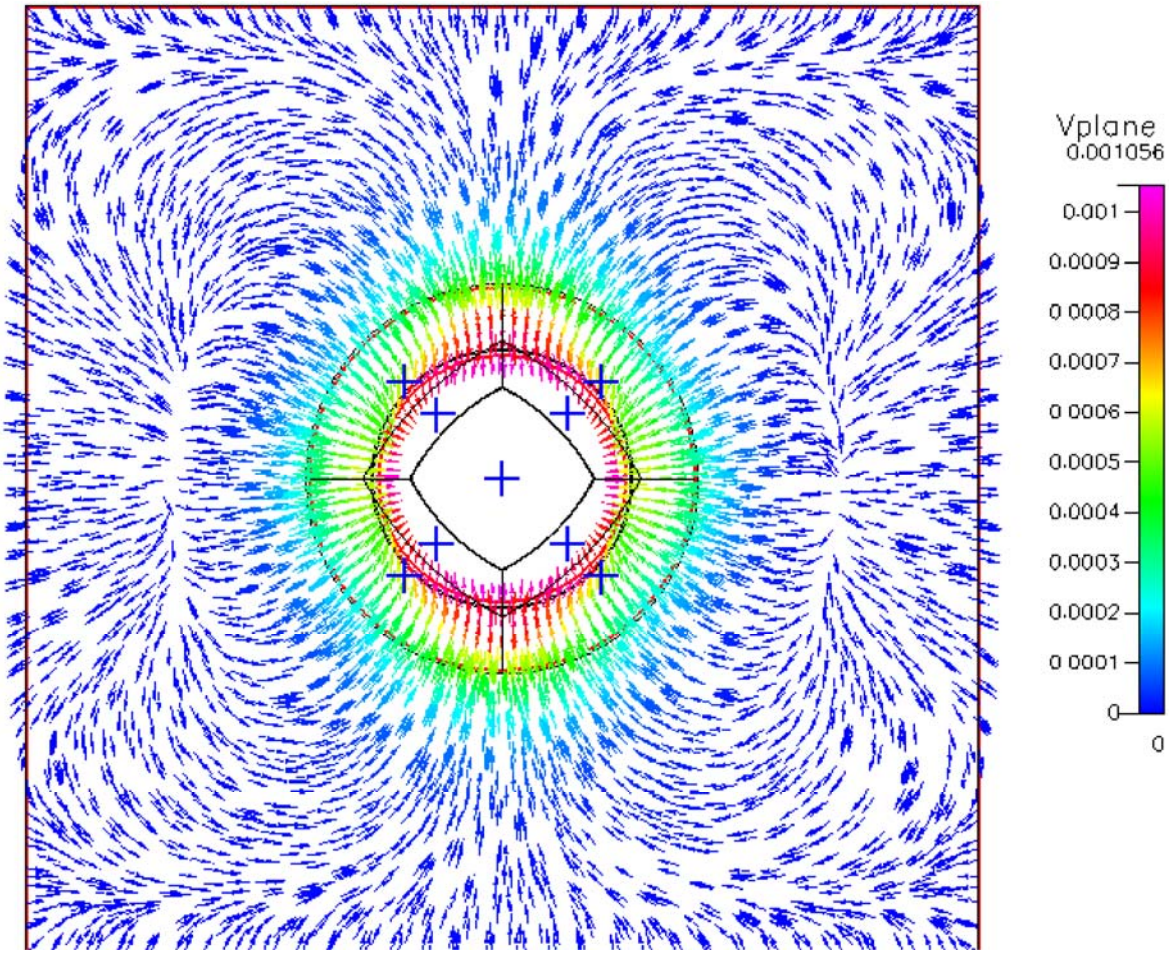

Fig. 3. Numerical results, z_1 plane. Velocity in *m/s*.

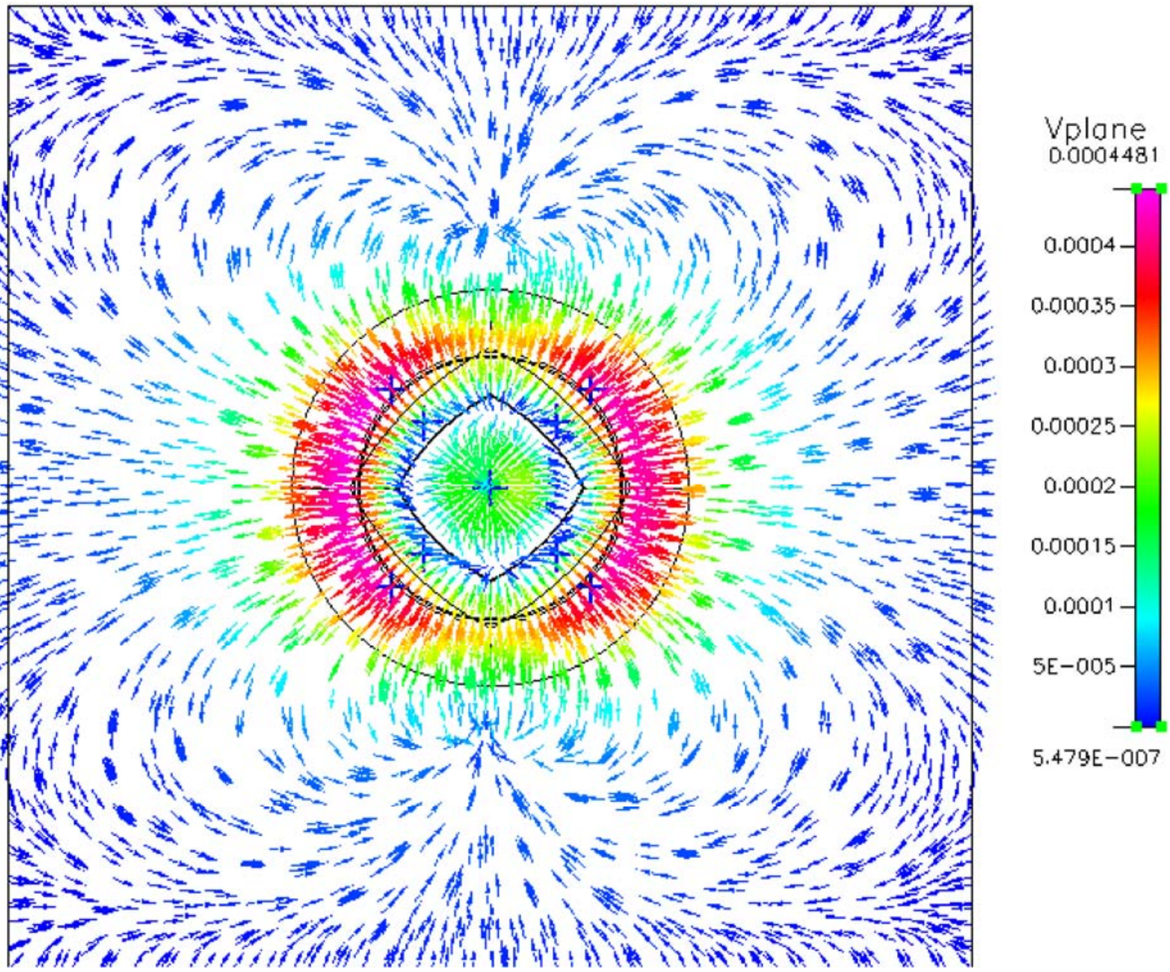

Fig. 4. Numerical results, z_2 plane. Velocity in *m/s*.

4.2. Grid Independence

In order to quantify the effect of the grid size on the numerical results, a grid independence study was undertaken, based on the models of Tho *et. al.*'s geometry. In this study, models with the same geometry and boundary conditions, but different grid sizes were analyzed. The numerical results in the same plane are shown for the three models in Figs. 5, 6 and 7. It is seen that all have the same overall flow structure, but there is significant differences in the location of the key features of the flow between model A and model B. Models B and C show much greater equivalence.

Model A has a maximum flow magnitude of 2.27 mm/s, model B 3.23 mm/s and model C 3.01 mm/s. The difference in flow velocity magnitude between model A and B is 30% and that between B and C is 7 %. Since the flow is at its maximum velocity only in a small volume, some variation in calculated maximum flow velocity is expected, depending on the exact location of the grid cells in the model.

From the results of the three models, it appears that to attain grid independence, a finer grid is needed than that used in model A, but that model B is sufficiently fine, since the results with a still finer grid are largely equivalent. Model B uses an average grid volume of 1.15 μm^3 in the momentum addition layer, for a bubble of radius 270 μm.

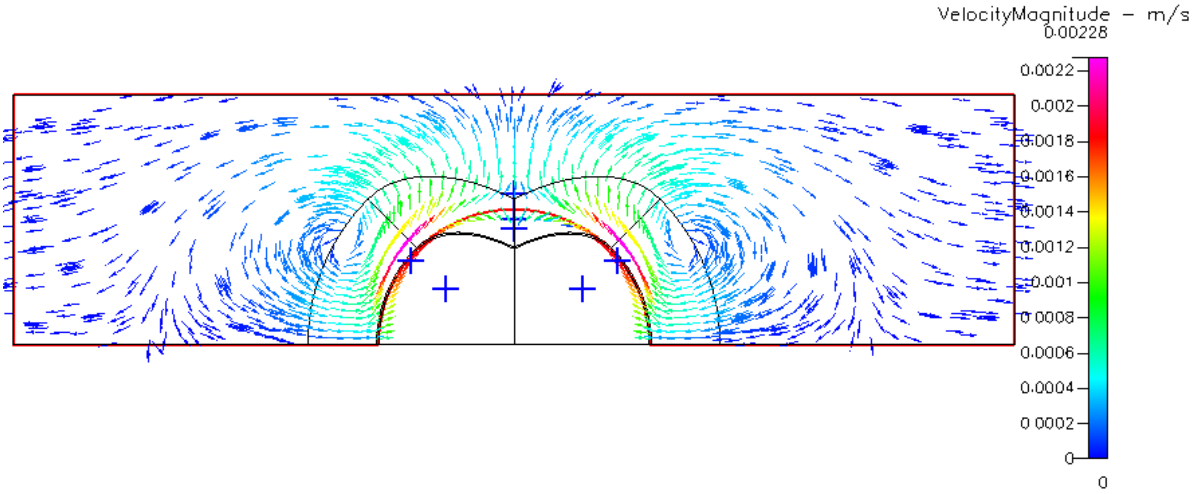

Fig. 5. Numerical results of Grid Independence model A.

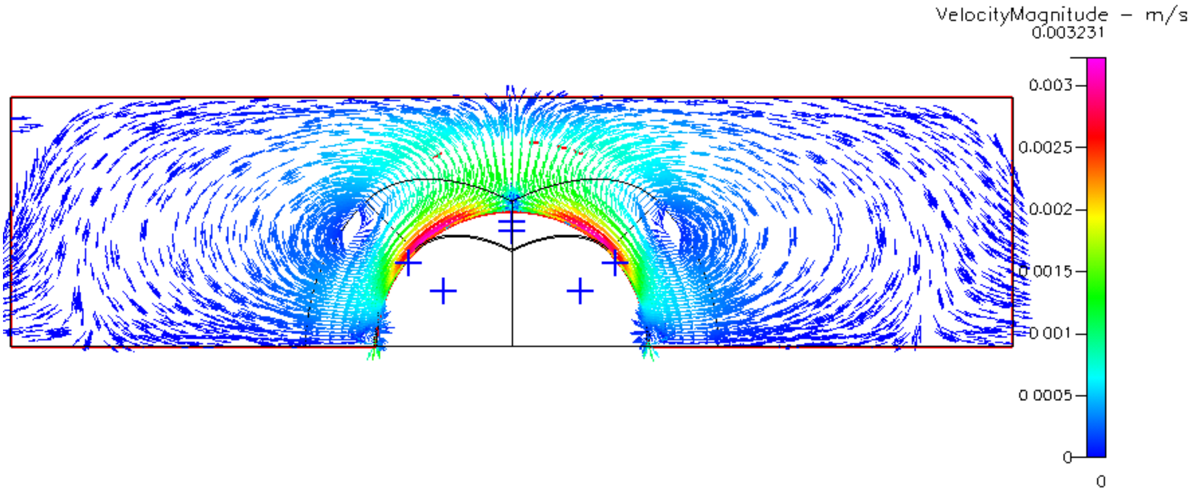

Fig. 6. Numerical results of Grid Independence model B.

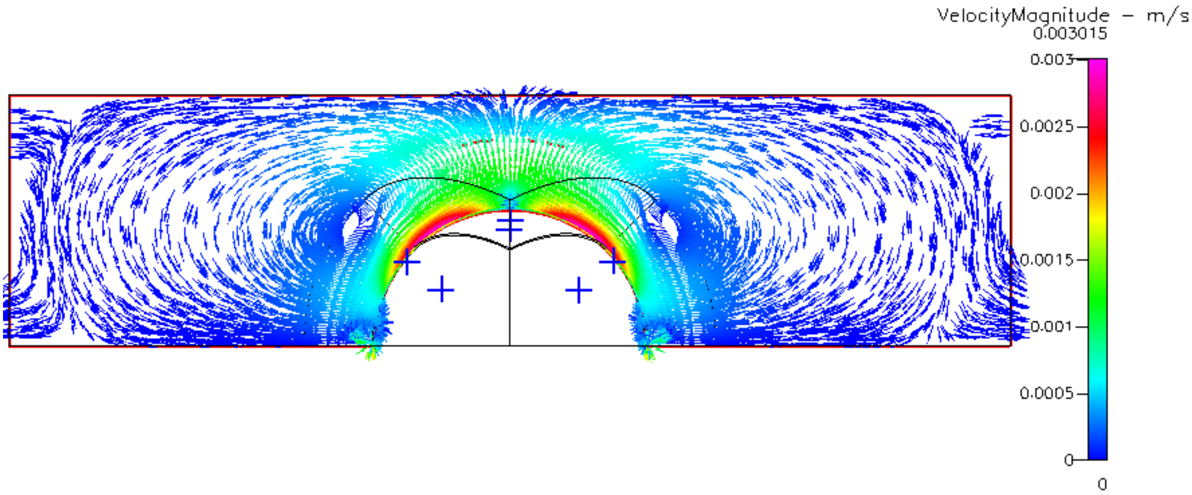

Fig. 7. Numerical results of Grid Independence model C.

4.3 Forcing Away from the Bubble

Marmottant *et. al.'s* assumption of the thickness of the viscous boundary layer [4] arises from a simplification of the first order flow equations. These equations are solved directly by the solver in the first order CFD model. This allows the validity of the assumption of a thin, constant thickness viscous boundary layer surrounding the bubble to be tested by calculating the forcing in all cells in the fluid volume, and observing how the magnitude of the forcing changes away from the bubble wall. The results for this for the CFD model representing Tho *et. al.*'s geometry [1] is shown in Fig. 8, which presents the forcing per unit volume against distance from the bubble wall, with each point plotted representing the average of the forcing in 100 cells.

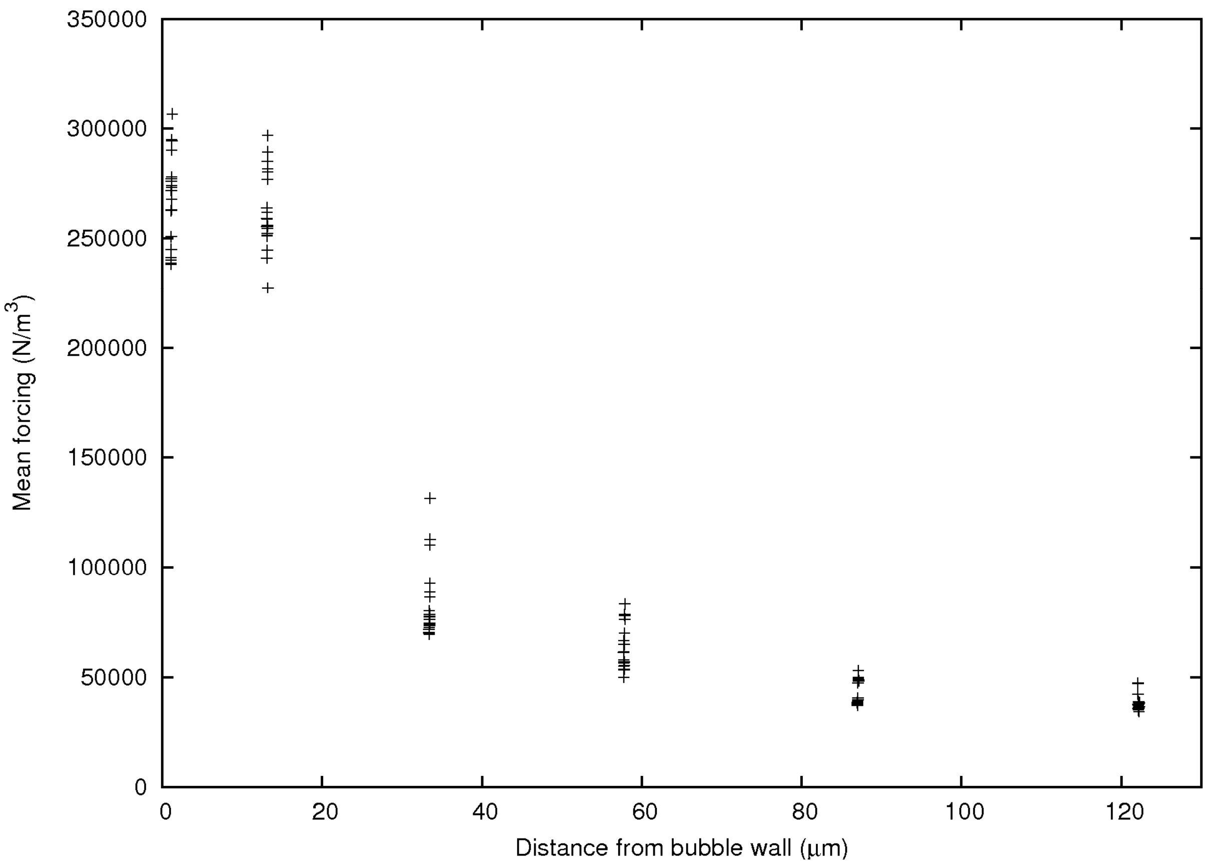

Fig. 8. The trend of volumetric forcing away from the bubble wall. Each point represents mean of 100 grid cells.

A clear trend can be seen where the forcing drops rapidly from around 300 kN/m^3 at the bubble wall to 50 kN/m^3 by 100 μm away from the bubble wall.

These results show that the forcing for the second order flow can be considered significant over a thickness of approximately 50 μm, compared to the thickness of 4.0 μm predicted by Marmottant *et. al.*'s approximation for these conditions [4]. However, the biggest portion of the forcing is within 15 μm of the bubble wall. The thickness where the forcing is active is still thin compared to the model size. This allows the calculation of forcing to be undertaken rapidly, as only a small volume requires its calculation. For improved results, the forcing should be calculated over a thickness between 3 and 10 times the viscous boundary layer thickness approximation.

The calculation of the forcing away from the bubble also allows the performance of the numerical differentiation method to be compared in the regular grid around the bubble and in the unstructured grid making up the remainder of the fluid volume. The method has previously been tested by using same grid as used for the fluid models, but applying values of a known analytical function to the grid. This allows the derivatives at each grid point to be calculated analytically, compared against the results of the numerical differentiation. This showed very good correlation when the method is applied to the regular grid, but poorer correlation in the scattered data field arising from the unstructured grid.

When the forcing is calculated for the whole fluid volume as shown in Fig. 9, at the interface between the regular grid and the unstructured grid, there is seen to be a significant discontinuity, where the calculated forcing in the unstructured grid is higher than that calculated in the adjacent regular grid. Due to the previous validation, it is thought that the forcing calculated in the regular grid is more accurate, and that the increase in the unstructured grid is due to the difficulty of numerical differentiation in the unstructured grid with the simple method used. There is of course no step difference in the flow or fluid properties between the regular and unstructured grid volumes.

In order to improve the calculation of the forcing on an unstructured grid, if required, a numerical differentiation method implementing the central difference method in three dimensions should be applied. As the forcing is only significant in the volume modelled with a regular grid, it is not thought that this differentiation problem causes significant difficulties with the models analyzed.

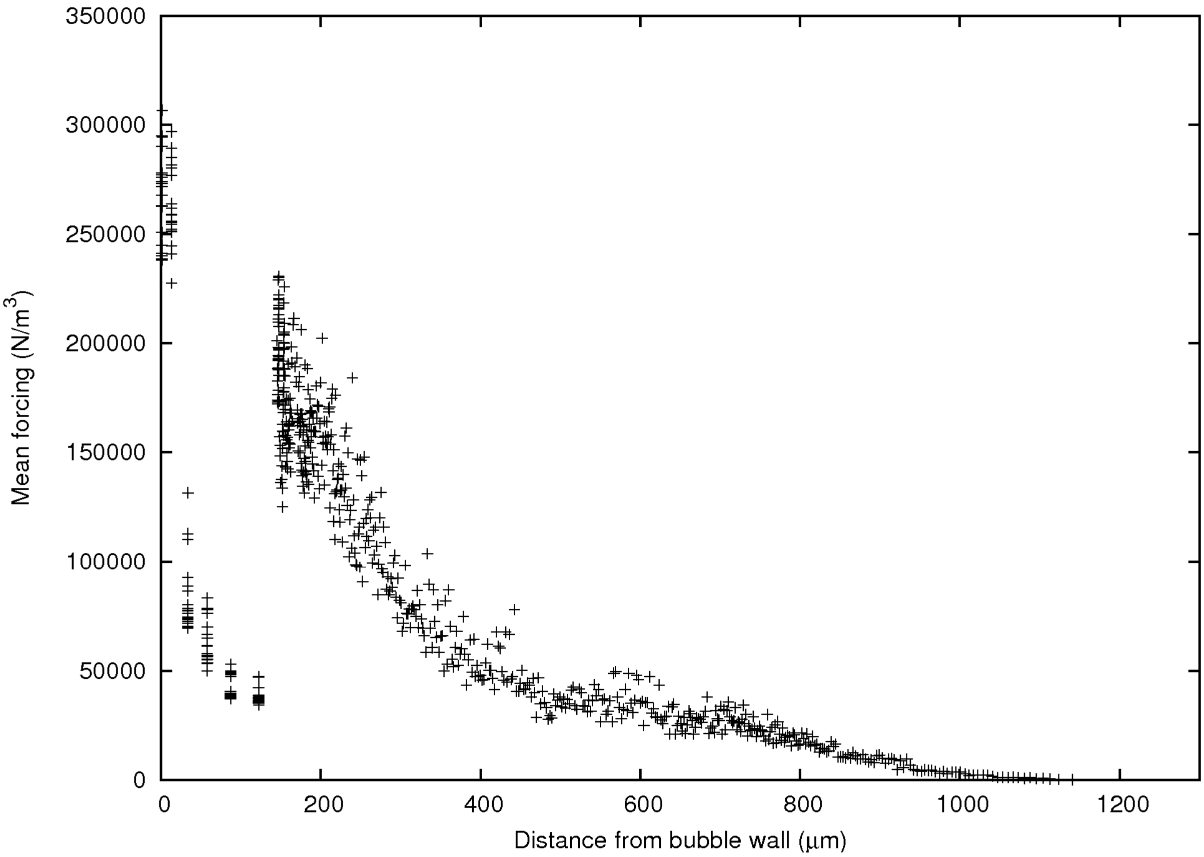

Fig. 9. Calculated volumetric forcing for the entire fluid volume, showing discontinuity in calculated forcing between regular grid and unstructured grid parts.

5. Conclusion

The multiscale modelling method described can predict the magnitude of steady streaming flows induced by bubble oscillation to within one order of magnitude. Due to the complex nature of both the pressure field and bubble motion in a real forced oscillation fluid/bubble system, the method, at its current state of development, cannot capture the fine details of the flow patterns that will be generated. This can be improved by computing a first order model which accurately accounts for both the gas bubble, the fluid and the interaction between them generated by an ultrasonic pressure wave. The principles of the numerical calculation of the forcing for the steady flow would remain as set out, but the technique could be improved by considering the forcing in a layer thicker than the viscous boundary layer thickness approximation.

Acknowledgements

The authors would like to acknowledge Mr Christopher Fenelly for his contributions to early development work on this methodology. JP and YV are grateful to the ESI Group and Dr. M. Megahed for allowing the use of the *CFD-ACE suite* in this study. We would also like to thank Mr B. Hibbert for volunteering additional computational resources for this study.

References

[1]. P. Tho, R. Mannasseh and A. Ooi, Cavitation microstreaming patterns in single and multiple bubble systems, *J. Fluid Mech.*, 576, 2007, pp. 191-233.
[2]. J. Xu and D. Attinger, Control and ultrasonic actuation of a gas-liquid interface in a microfluidic chip, *J. Micromech. Microeng.*, 17, 2007, pp. 609-616.
[3]. J. Lighthill, Acoustic Streaming, *J. Sound Vib.*, 63, 3, 1978, pp. 391-418.
[4]. P. Marmottant, J. P. Raven, H. Gardeniers, J. G. Bomer and S. Hilgenfeldt., Microfluidics with ultrasound-driven bubbles, *J. Fluid Mech.*, 568, 2006, pp. 109-118.
[5]. C. P. Lee and T. G. Wang, Outer acoustic streaming, *J. Acoust. Soc. Am.*, 88, 5, 1990, pp. 2367-2375.

Guide for Contributors

Aims and Scope

Sensors & Transducers Journal (ISSN 1726-5479) provides an advanced forum for the science and technology of physical, chemical sensors and biosensors. It publishes state-of-the-art reviews, regular research and application specific papers, short notes, letters to Editor and sensors related books reviews as well as academic, practical and commercial information of interest to its readership. Because it is an open access, peer review international journal, papers rapidly published in *Sensors & Transducers Journal* will receive a very high publicity. The journal is published monthly as twelve issues per annual by International Frequency Association (IFSA). In additional, some special sponsored and conference issues published annually. *Sensors & Transducers Journal* is indexed and abstracted very quickly by Chemical Abstracts, IndexCopernicus Journals Master List, Open J-Gate, Google Scholar, etc.

Topics Covered

Contributions are invited on all aspects of research, development and application of the science and technology of sensors, transducers and sensor instrumentations. Topics include, but are not restricted to:

- Physical, chemical and biosensors;
- Digital, frequency, period, duty-cycle, time interval, PWM, pulse number output sensors and transducers;
- Theory, principles, effects, design, standardization and modeling;
- Smart sensors and systems;
- Sensor instrumentation;
- Virtual instruments;
- Sensors interfaces, buses and networks;
- Signal processing;
- Frequency (period, duty-cycle)-to-digital converters, ADC;
- Technologies and materials;
- Nanosensors;
- Microsystems;
- Applications.

Submission of papers

Articles should be written in English. Authors are invited to submit by e-mail editor@sensorsportal.com 8-14 pages article (including abstract, illustrations (color or grayscale), photos and references) in both: MS Word (doc) and Acrobat (pdf) formats. Detailed preparation instructions, paper example and template of manuscript are available from the journal's webpage: http://www.sensorsportal.com/HTML/DIGEST/Submition.htm Authors must follow the instructions strictly when submitting their manuscripts.

Advertising Information